PCCP

PAPER

View Article Online
View Journal | View Issue

Cite this: *Phys. Chem. Chem. Phys.*, 2024, **26**, 16597

Localized surface plasmon resonances of size-selected large silver nanoclusters (n = 70–100) soft-landed on a C_{60} organic substrate†

Tomoya Inoue,[a] Kaito Mizoguchi,[a] Miwa Tokita,[a] Masahiro Shibuta,‡[b] Masato Nakaya,§[a] Toyoaki Eguchi¶[a] and Atsushi Nakajima *[ab]

Received 18th March 2024,
Accepted 22nd May 2024

DOI: 10.1039/d4cp01151a

rsc.li/pccp

Silver nanoclusters (Ag_n NCs) exhibit a remarkable optical property known as localized surface plasmon resonance (LSPR) in the visible to ultraviolet wavelengths. In this study, we address the size gap in LSPR responses between small NCs and nano-islands by synthesizing large Ag_n NCs with a countable number of atoms (n = 70–100) using a magnetron sputtering method, which were precisely size-selected and soft-landed onto substrates. The monodispersed Ag_n NCs were immobilized on a pre-decorated substrate with fullerene (C_{60}) molecules, and their LSPR behaviors were characterized using two-photon photoemission (2PPE) spectroscopy. Due to the distinct polarization selectivity of incident light associated with LSPR, the intensity ratio between p- and s-polarized lights (I_p/I_s) in 2PPE spectroscopy serves as a reliable indicator of LSPR and its structural correlations. From n = 70 to 100, the I_p/I_s value gradually decreases as the cluster size increases. This decrease is attributed to the enhancement of s-polarized light (I_s), indicating that large Ag_n NCs on a C_{60} substrate undergo a deformation from spherical to flattened geometries, particularly above approximately n = 55.

Introduction

The intense light absorption resulting from collective photo-excitation in assemblies of metal atoms is known as localized surface plasmon resonance (LSPR), where the optical response of LSPR varies with the size, composition, structure, and surrounding environment of the metal assemblies.[1–4] Silver (Ag), belonging to the Group 11 elements, efficiently converts ultraviolet-visible light into excitons through LSPR, and due to its chemical stability, numerous applications combining Ag LSPR with light excitation processes have been experimentally explored.[5–12] The optical responses in large nanoparticles with sizes of around 100 nm can be theoretically explained within the framework of classical electromagnetism, approximated with continuous band structures.[13]

Conversely, LSPR responses have been observed in the gas phase even in countable nano-sized regions containing a few to a few hundred atoms, corresponding to nanoclusters (NCs) with diameters below a few nanometers.[14–19] These findings have spurred research into constructing a theoretical framework based on quantum theory calculations, to enhance our understanding of the optical responses in these NC regions.[20–29] Regarding the threshold size for LSPR optical response in a NC, the LSPR response of Ag_n NCs emerges at around 9 atoms when fabricating size-selectively monodispersed Ag_n NCs on a C_{60} organic substrate. Two-photon photoemission (2PPE) spectroscopy elucidates the LSPR response, showcasing polarization-dependent enhanced photoemission, including wavelength dependence and electronic relaxation processes of massive flat-shaped Ag NCs on graphite substrates.[9,10,30] However, there exists a size gap in the research between small NCs up to approximately 50 atoms and flat-shaped NC islands with hundreds of atoms. It is therefore essential to evaluate the optical properties using atomically precise Ag_n NCs monodispersed on a substrate to spectroscopically reveal the transition regions for advancing theoretical treatments.

In this study, large Ag_n NCs (n = 70, 85, and 100) were uniformly surface-immobilized on organic C_{60} substrates, and their LSPR responses were evaluated using 2PPE spectroscopy. We will discuss the correlation with surrounding environments

[a] *Department of Chemistry, Faculty of Science and Technology, Keio University, 3-14-1 Hiyoshi, Kohoku-ku, Yokohama 223-8522, Japan.*
E-mail: nakajima@chem.keio.ac.jp; Fax: +81-45-566-1697; Tel: +81-45-566-1712
[b] *Keio Institute of Pure and Applied Sciences (KiPAS), Keio University, 3-14-1 Hiyoshi, Kohoku-ku, Yokohama 223-8522, Japan*

† Electronic supplementary information (ESI) available. See DOI: https://doi.org/10.1039/d4cp01151a

‡ Present address: Department of Physics and Electronics, Graduate School of Engineering, Osaka Metropolitan University, 1-1 Gakuen-cho, Naka-ku, Sakai, Osaka 599-8531, Japan.
§ Present address: Department of Energy Science and Engineering, Nagoya University, Furo-cho, Chikusa-ku, Nagoya 464-8603, Japan.
¶ Present address: The Toyama Monozukuri Center, 3816-1 Kishi, Yamakita-machi, Ashigarakami-gun, Kanagawa, 258-0112, Japan.

and structures by comparing them with classical optical-electromagnetic field analyses.[31]

Experimental and calculation details

NC synthesis

Experimental details have been previously published.[12,30,32–34] Briefly, Ag_n NCs were synthesized in the gas phase using a magnetron sputtering (MSP) system (NAP01-nanojima, Ayabo Corp.). After mass selection using a quadrupole mass analyzer (MAX-16000, Extrel CMS), the Ag atoms and ions ejected by accelerating Ar^+ ions from a Ag target were cooled and aggregated in helium (He) gas at liquid nitrogen temperature. The Ag_n NCs were then grown within the growth cell cooled by liquid nitrogen. The Ag_n NC cations generated in the growth cell were selectively transported using a quadrupole ion guide and an ion deflector, and then introduced into the quadrupole mass analyzer for precise mass selection on a single-atom basis. The synthesis conditions of Ag_n NCs were optimized while detecting the ion current originating from Ag_n NC cations after mass separation to obtain the targeted size n of NCs. The deposition of Ag_n NC cations was carried out by applying a sufficiently low negative voltage of −5 V to the sample substrate to gently attract positive ions, ensuring soft-landing conditions where the NCs are not destroyed upon collisions with the substrate, and deposited 0.2 monolayer (ML) under these conditions. A highly purified HOPG substrate heated to 400 °C and pre-coated with a 2 ML C_{60} film was used as the sample substrate. The Ag NC-supported substrate was transferred to the photoemission spectroscopy system under ultra-high vacuum conditions ($\sim 10^{-8}$ Pa). Furthermore, the monodispersity of Ag_n NCs on the C_{60} substrate was confirmed in advance using a scanning tunneling microscope (STM), the images of which were analyzed using WSxM software.[35]

2PPE measurements

In this study, measurements were conducted using 2PPE spectroscopy, where the incident light served as both pump and probe light.[12,30,36] For 2PPE, second and third harmonics (SH and TH) obtained from a Ti:sapphire laser (COHERENT, Mira-900F; 76 MHz, 150 fs) were used, resulting in photon energy ranges of 2.26–3.44 eV and 3.96–4.65 eV, respectively. The incident light was focused onto the sample using an aluminum-coated concave mirror (f = 400 mm), and the incident angle was set to 65°. The polarization of the incident light was changed to p-polarization and s-polarization in the vertical and horizontal directions of the substrate, respectively, using a half-wave plate. The kinetic energy distributions of photoelectrons generated by the two-photon process using polarized light were detected using a hemispherical electron energy analyzer (VG SCIENTA, R-3000), and the sample temperature during measurements was maintained at 293 K.

Optical-electromagnetic field analysis

The optical absorption efficiencies of metal spheres supported as complete spheres and truncated spheres on dielectric films were calculated using a model based on classical electromagnetism by M. M. Wind *et al.*[31] The dielectric function of Ag was used for the metal spheres,[37] a value of 4.0 was employed for the dielectric constant of C_{60} as the support material,[38,39] and the surrounding medium was assumed to be vacuum (ε = 1.0). The radius of the metal spheres, r, was set to 0.8 nm, and simulations were conducted for both complete spheres (θ = 180°) and truncated spheres (θ = 135°).

Results and discussion

2PPE spectrum of Ag_{100}/C_{60}

Fig. 1 shows the STM image obtained when depositing Ag_{75} NCs. From the figure, it is evident that each Ag_n NC is immobilized in a monodispersed state on the C_{60} substrate. The height on the C_{60} surface averages around 1.3 nm, which is notably higher than 0.8 nm height reported previously for Ag_{13} but is comparable to the average height of Ag_{55}, also reported as 1.3 nm.[32] Regarding the lateral width, the differences depending on the shape of the STM tip are significant, making quantitative comparisons difficult. From this monodispersed state, it is confirmed that the optical response is defined by Ag_n NCs with a precise number of atoms, as demonstrated in Fig. S1 in the ESI† for smaller sized Ag_n on a C_{60} substrate. Ultraviolet and X-ray photoelectron spectra for large Ag_n NCs on a C_{60} substrate are provided in Fig. S2 in the ESI.†

Fig. 2(a) shows the 2PPE spectrum of Ag_{100} NCs (0.2 ML) on a C_{60} substrate measured with p-polarization (red) and s-polarization (blue) at $h\nu$ = 4.04 eV (TH photons). The photoemission yield detected with p-polarization is generally enhanced compared to that with s-polarization, particularly exhibiting an exponential increase in photoemission yield between 4.5 eV and 5.5 eV in a final energy from the Fermi level (E_F). This enhancement is attributed to the photoemission spectrum measurement encompassing electronic relaxation processes after LSPR excitation, where

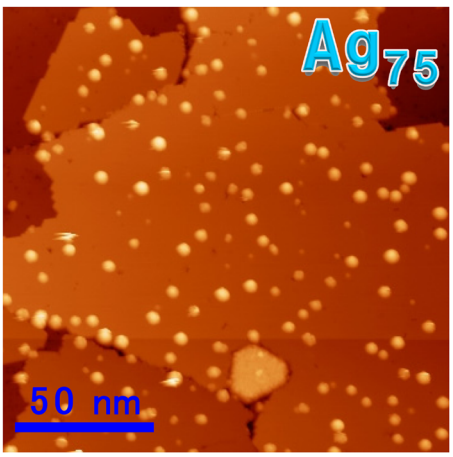

Fig. 1 STM image of soft-landed Ag_{75} NCs on a C_{60} substrate (160 × 160 nm^2) at a low coverage ($\sim 4 \times 10^3$ dots per $\mu m^2 \approx 7.3 \times 10^{-3}$ ML). The tip bias voltage (V_t) and tunneling current (I_t) are V_t = −2.0 V and I_t = 10 pA, respectively. Bright dots correspond to individual Ag_{75} NCs, monodispersively immobilized on the C_{60} surface, where the average height of Ag_{75} NCs is around 1.3 nm.

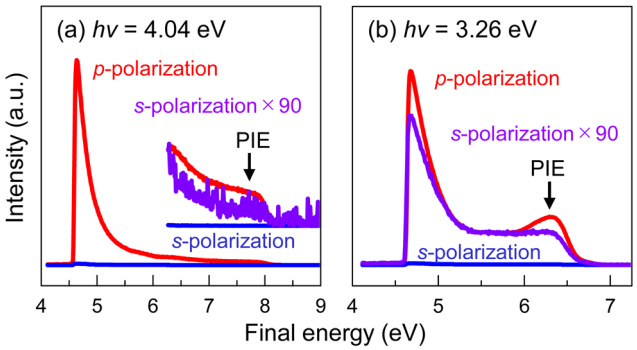

Fig. 2 2PPE spectra for the Ag_{100} NC (0.2 ML) deposited on a C_{60} substrate, captured with (a) $h\nu$ = 4.04 eV (TH photons) and (b) $h\nu$ = 3.26 eV (SH photons). The insets in (a) show magnified spectra in the high energy region of 6.3–9.0 eV. Following the deposition of Ag_{100} NCs, the 2PPE intensities are noticeably enhanced, accompanied by broad PIE spectral features extending to approximately $E_F + 2h\nu$ in both (a) and (b). The 2PPE spectrum with *s*-polarized light (purple), scaled by a factor of about 90, aligns with the spectrum obtained with *p*-polarized light (red), showing that the PIE of *p*-polarized light is 90 times stronger than that of *s*-polarized light (blue).

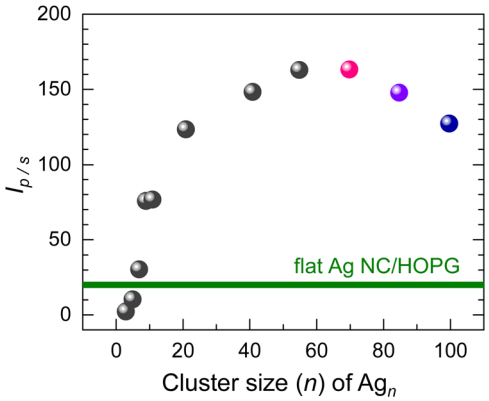

Fig. 3 The I_p/I_s values of Ag_n NCs deposited on a C_{60} substrate are plotted against cluster size *n*. These I_p/I_s values are determined by integrating the PIE (>6 eV region in final energy) from the 2PPE spectra of SH photons at $h\nu$ = 3.26 eV for both *p*- and *s*-polarization. Based on the I_p/I_s values, the plasmonic response of Ag_n NCs becomes evident at $n \geq 9$ and reaches a local maximum around n = 60, followed by a gradual decline; three colored dots in pink, violet and blue represent Ag_n NCs (n = 70, 85, and 100), respectively, while the other dots in black correspond to values reported previously.[30] For ref. 10, an I_p/I_s value of 20 is indicated for flat-shaped Ag NCs ($\varphi \sim 2.5$ nm, $t \sim 1$ nm, $n \sim 8 \times 10^2$) on HOPG at $h\nu$ = 3.26 eV, represented by a green line.

low-energy hot electrons are generated to approach thermal equilibrium distribution through the Landau damping (1–100 fs) and exciton relaxation processes (100 fs–1 ps).[9,10,30,40]

Additionally, as shown in Fig. 2(a), a peak attributed to LSPR excitation, PIE (photoemission intensity enhancement), is observed around $E_F + 2\ h\nu$ (*ca.* 8 eV in final energy), where the photoemission yield is more than 90 times larger with *p*-polarization (red) than with *s*-polarization (purple). A similar trend is observed in Fig. 2(b) for the 2PPE spectrum measured with $h\nu$ = 3.26 eV (SH photons), where the photoemission intensity with *p*-polarization (red) is also more than 90 times larger than that with *s*-polarization (purple), particularly exhibiting a significant increase in photoelectrons below 5.0 eV and above 6.0 eV of final energy in the PIE region.

Size dependence of I_p/I_s

To quantitatively evaluate the LSPR response, the ratio of photoemission intensity with *p*-polarization to that with *s*-polarization is defined in the PIE region as I_p/I_s, and its size dependence at $h\nu$ = 3.26 eV is shown in Fig. 3. The reported I_p/I_s values for Ag_n NCs on C_{60} substrates with $n \leq 55$ (black circles) are included to observe their size evolution,[30] along with that for flat-shaped Ag_n NCs on HOPG substrates with $\varphi \sim 2.5$ nm, $t \sim 1$ nm (n is roughly estimated to 8×10^2) (green line) reported by S. Tan *et al.*[10]

Regarding the size evolution from Ag_3 atom to Ag_{100}, I_p/I_s increases at small size n, reaching a threshold around $n \sim 9$, then peaking around $n \sim 60$ with further size increase, and subsequently shows a monotonic decrease for larger sizes. Notably, I_p/I_s begins to decrease for larger sizes with $n > 55$, eventually converging to a small I_p/I_s value. This trend can be rationalized by considering that I_p/I_s at $h\nu$ = 3.26 eV for flat Ag NCs with sizes around $n \sim 8 \times 10^2$ supported on HOPG substrates has been reported as a small I_p/I_s value of 20. However, it is unlikely that the LSPR response itself reaches a maximum at $n \sim 60$, as it has been reported that LSPR absorption efficiency further increases toward particle sizes of 20 nm or larger ($n > 2 \times 10^5$).[41,42]

Photon energy dependence in *p*- and *s*-polarizations

To elucidate the reason for the decrease in I_p/I_s value with increasing size n, the 2PPE spectra were measured with varying photon energies in *p*-polarization for Ag_n (n = 70, 85, and 100), and the relative intensity in the PIE region is plotted in Fig. 4. The intensity increases towards 3.6–3.7 eV, similar to Ag_n NCs/C_{60} with $n \leq 55$, and no distinct shift in the center wavelength of LSPR is observed with size variation. However, particularly in the SH wavelength region with $h\nu < 3.5$ eV, the intensity of I_p decreases from n = 70 to n = 85 for the same photon energy.

Next, to investigate the behaviors with I_s, the 2PPE spectra were measured with varying photon energies in *s*-polarization for Ag_n NCs (n = 21, 55, 70, and 100), and the relative intensity in the PIE region is plotted in Fig. 5. For Ag_{21} and Ag_{55}, there is no discernible photon energy dependence, and no distinct structures in I_s are observed. On the other hand, for larger sizes such as Ag_{70} and Ag_{100}, an increase in intensity in I_s is observed in the range of $h\nu$ = 3.0–3.4 eV, showing a peak-like structure around $h\nu \sim 3.2$ eV. The result suggests that the decline in I_p/I_s with size for $n > 55$, observed in Fig. 3 at $h\nu$ = 3.26 eV, is attributable to both a decrease in I_p and an increase in I_s.

Classical electromagnetic field analysis for photo-absorption of Ag_{100}/C_{60}

To investigate the origin of the observed peak in the photon energy dependence of 2PPE intensity at *s*-polarization, an optical electromagnetic field simulation was conducted for

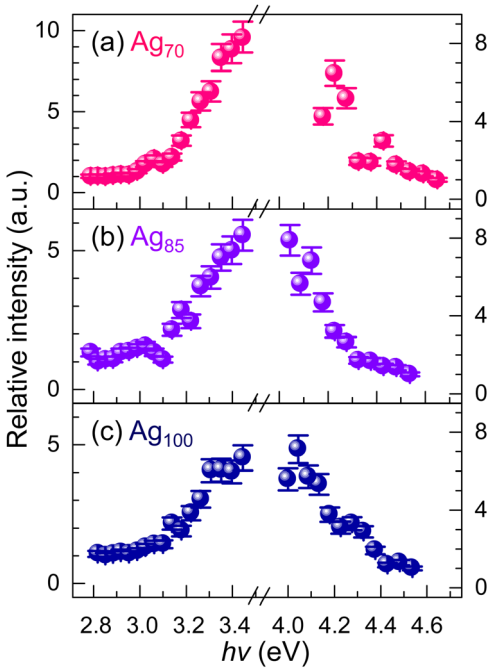

Fig. 4 PIE intensities integrated from $E_F + 2h\nu$ to $E_F + 2h\nu - 0.5$ eV for three sizes of Ag_n NCs (n = 70, 85, and 100) against $h\nu$ in p-polarization. The peak of PIE intensities could not be observed with the $h\nu$ window of the SH and TH photons in this study.

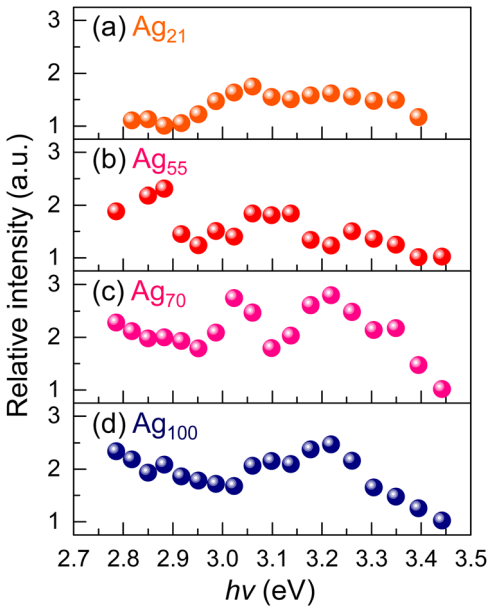

Fig. 5 Photon energy dependence of photoemission in Ag_n/C_{60} (n = 21, 55, 70, and 100), measured with s-polarized light within the range of 2.77 to 3.45 eV. Above n = 70, photoemission enhancements with s-polarized light are observed, resulting in a decrease in I_p/I_s values.

the Ag_{100}/C_{60} system. Fig. 6 illustrates the normalized absorption cross-sections for the substrate in horizontal and vertical (surface normal) directions when Ag_{100} NC is assumed to be supported on the C_{60} substrate; (a) a truncated sphere and (b) a complete sphere. In the simulation, a dielectric constant of 4.0 was used for the C_{60} substrate[38,39] and the experimentally measured dielectric constant was used for the Ag metal film.[37] Two spherical Ag_{100} shapes are assumed with a radius of 0.8 nm; (a) truncated at θ = 135° from the apex and (b) untruncated (θ = 180°), as shown in the insets of Fig. 6. In the case of the truncated sphere (a), the LSPR absorption (red) in the substrate vertical direction (p-polarization) is observed at 3.4 eV, which is 0.2–0.3 eV lower than the experimentally measured value. This discrepancy is likely due to the simulation's accuracy being limited to classical analysis, and further discussion is needed to include quantum size effects.[43,44] On the other hand, the LSPR absorption (blue) in the substrate horizontal direction (s-polarization) is observed at a lower energy of 2.9 eV, which is 0.5 eV lower than the absorption in the substrate vertical direction (red). This qualitatively reproduces the experimental results shown in Fig. 5(d).

In the case of the complete sphere (b), conversely, LSPR absorption in the substrate horizontal direction (blue) is calculated to occur on the higher energy side compared to the substrate vertical direction (red). This discrepancy does not align the experimental results indicating the appearance of lower energy components. These analyses suggest that the low energy components responsible for s-polarized light are attributed to a flattened structure of Ag_n NCs with $n > 55$, similar to a truncated sphere. Furthermore, the lower intensity I_p in p-polarization for n = 70 compared to n = 85 and 100 can be explained by the shorter distance in the substrate vertical direction (lower height) in Ag_n NCs deformed by flattening. While the LSPR response in the NC region increases with distance in the substrate vertical direction,[23,25,26] the diameter of n = 55, which is considered close to a complete sphere based on STM,[32] is 1.2 nm, which is almost the same as the vertical length of 1.3 nm in the truncated sphere of n = 100. Specifically, such flattening deformation of supported Ag NCs with increasing size has also been reported on silica glass substrates,[8,9] and thus the decrease in I_p/I_s at $h\nu$ = 3.26 eV for Ag_n NCs with $n > 55$ in this study is attributable to the formation of a flattened structure of Ag_n NCs on the C_{60} substrate. Namely, a flattened structure of larger Ag_n NCs could result in the manifestation of LSPR absorption in s-polarization and a decrease in distance in the substrate vertical direction.

Previous theoretical studies have shown that the magnitude of the LSPR transition moment is proportional to the particle size in regions of NCs.[25] When 55-mer and 100-mer nanoclusters are supported on a C_{60} organic substrate as complete or truncated spheres, respectively, as shown in Fig. 6(b) and (a), respectively, the vertical dimension relative to the substrate remains the same for both clusters (1-fold), while the maximum horizontal length is 1.2 times longer for the 100-mer compared to the 55-mer. In fact, 2PPE measurements indicate that the I_p/I_s ratio for the 55-mer is 1.3 times larger than for the 100-mer, suggesting flattening deformation in the 100-mer.

The optical response of LSPR is influenced by the mode of excitation and precise atomic configurations, which are essential for maximizing the atomic utilization of precious metals.

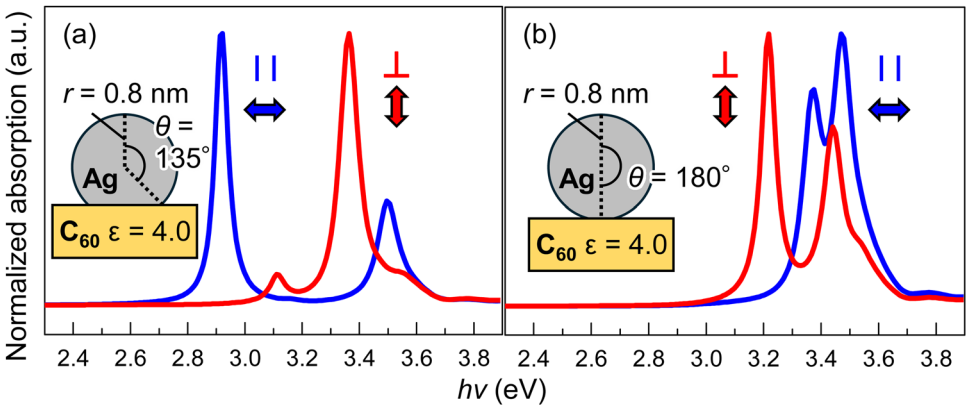

Fig. 6 Photoexcitation simulation of absorption efficiency for Ag_{100} supported as (a) cut spheres or (b) perfect spheres on C_{60} using a classical electromagnetic model. When the photoexcitation is perpendicular to the substrate (*p*-polarized light), the absorption peak is observed at 3.4 eV, while with the horizontal direction (*s*-polarized light), the absorption peak shifts to 2.9 eV, which represents a decrease of 0.5 eV in (a). On the other hand, in (b) photoexcitation of the perpendicular direction shows lower energy than that of the horizontal direction.

By strategically positioning plasmonic particles on solid surfaces, improvements in optical materials like photocatalysts and solar cells are expected with minimal additions. However, there is limited research on how the size and shape of nanoclusters affect plasmonic functionality. This study explores the relationship between plasmonic responses and structural changes in silver nanoclusters, offering important insights that could refine plasmonic device functions. The findings provide critical guidelines for designing plasmonic systems and help bridge the gap between nanocluster science and mesoscopic plasmonics.

Conclusions

The LSPR response of large Ag_n NCs (n =70, 85, and 100) precisely immobilized on C_{60} substrates was evaluated using 2PPE. When irradiated with *p*-polarized light, the photoemission intensity increases dramatically compared to the intensity with *s*-polarized light, indicating a strong LSPR effect. However, the ratio of photoemission intensity between *p*- and *s*-polarized lights, I_p/I_s, gradually decreases with larger sizes, specifically for $n > 55$. The LSPR response in *s*-polarization becomes observable for these larger sizes, suggesting that Ag_n NCs adopt flattened structures on the C_{60} substrate, which is qualitatively consistent with optical electromagnetic field simulation based on classical models. These results demonstrate that I_p/I_s serves as an indicator of LSPR, which sensitively responds to surface immobilization structures, allowing for the evaluation of the LSPR response of uniformly dispersed Ag_n NCs on dielectric films, including their structural correlations. The precise design of LSPR responses through structural control of Ag_n NCs deposited on different substrates and sizes is expected to contribute to the development of optoelectronic conversion materials based on plasmonic nanostructures.

Data availability statement

Data related to this work are available in the ESI.†

Conflicts of interest

The authors declare no competing financial interest.

Acknowledgements

This work is partly supported by JSPS KAKENHI of Grants-in-Aid for Scientific Research (A) No. 19H00890, for Challenging Research No. 21K18939, and for Transformative Research Areas (A) ''Hyper-Ordered Structures Science'' (21H05573).

References

1 U. Kreibig and M. Vollmer, *Optical Properties of Metal Clusters*, Springer, Berlin, 1995.
2 K. L. Kelly, E. Coronado, L. L. Zhao and G. C. Schatz, *J. Phys. Chem. B*, 2003, **107**, 668–677.
3 M. Rycenga, C. M. Cobley, J. Zeng, W. Li, C. H. Moran, Q. Zhang, D. Qin and Y. Xia, *Chem. Rev.*, 2011, **111**, 3669–3712.
4 E. Petryayeva and U. J. Krull, *Anal. Chim. Acta.*, 2011, **706**, 8–24.
5 A. J. Haes and R. P. Van Duyne, *J. Am. Chem. Soc.*, 2002, **124**, 10596–10604.
6 P. Christopher, H. Xin and S. Linic, *Nat. Chem.*, 2011, **3**, 467–472.
7 M. Valamanesh, Y. Borensztein, C. Langlois and E. Lacaze, *J. Phys. Chem. C*, 2011, **115**, 2914–2922.
8 M. Thämer, A. Kartouzian, P. Heister, T. Lünskens, S. Gerlach and U. Heiz, *Small*, 2014, **10**, 2340–2344.
9 S. Tan, A. Argondizzo, J. Ren, L. Liu, J. Zhao and H. Petek, *Nat. Photonics*, 2017, **11**, 806–812.
10 S. Tan, L. Liu, Y. Dai, J. Ren, J. Zhao and H. Petek, *J. Am. Chem. Soc.*, 2017, **139**, 6160–6168.
11 C. Liang, Z. A. Lu, J. Wu, M. X. Chen, Y. Zhang, B. Zhang, G. L. Gao, S. Li and P. Xu, *ACS Appl. Mater. Interfaces*, 2020, **12**, 54266–54284.

12 K. Yamagiwa, M. Shibuta and A. Nakajima, *ACS Nano*, 2020, **14**, 2044–2052.
13 G. Mie, *Ann. de. Phys.*, 1908, **25**, 377–445.
14 J. Tiggesbäumker, L. Köller, K. H. Meiwes-Broer and A. Liebsch, *Phys. Rev. A: At., Mol., Opt. Phys.*, 1993, **48**, R1749–R1752.
15 W. A. de Heer, *Rev. Mod. Phys.*, 1993, **65**, 611–676.
16 E. Loginov, L. F. Gomez, N. Chiang, A. Halder, N. Guggemos, V. V. Kresin and A. F. Vilesov, *Phys. Rev. Lett.*, 2011, **106**, 233401.
17 C. Xia, C. Yin and V. V. Kresin, *Phys. Rev. Lett.*, 2009, **102**, 156802.
18 S. Kawamura, M. Yamaguchi, S. Kono, M. Arakawa, T. Yasuike, T. Horio and A. Terasaki, *J. Phys. Chem. A*, 2023, **127**, 6063–6070.
19 N. Iwe, K. Raspe, F. Martinez, L. Schweikhard, K.-H. Meiwes-Broer and J. Tiggesbäumker, *Phys. Chem. Chem. Phys.*, 2023, **25**, 1677–1684.
20 V. Bonačić-Koutecký, L. Češpiva, P. Fantucci, J. Pittner and J. Koutecký, *J. Chem. Phys.*, 1994, **100**, 490–506.
21 K. Yabana and G. F. Bertsch, *Phys. Rev. A: At., Mol., Opt. Phys.*, 1999, **60**, 3809–3814.
22 E. Cottancin, G. Celep, J. Lermé, M. Pellarin, J. R. Huntzinger, J. L. Vialle and M. Broyer, *Theor. Chem. Acc.*, 2006, **116**, 514–523.
23 J. Yan, Z. Yuan and S. Gao, *Phys. Rev. Lett.*, 2007, **98**, 216602.
24 G.-T. Bae and C. M. Aikens, *J. Phys. Chem. C*, 2012, **116**, 10356–10367.
25 T. Yasuike, K. Nobusada and M. Hayashi, *Phys. Rev. A: At., Mol., Opt. Phys.*, 2011, **83**, 013201.
26 T. Yasuike and K. Nobusada, *Phys. Chem. Chem. Phys.*, 2013, **15**, 5424–5429.
27 E. B. Guidez and C. M. Aikens, *Nanoscale*, 2014, **6**, 11512–11527.
28 M. Kuisma, A. Sakko, T. P. Rossi, A. H. Larsen, J. Enkovaara, L. Lehtovaara and T. T. Rantala, *Phys. Rev. B: Condens. Matter Mater. Phys.*, 2015, **91**, 115431.
29 R. Schira and F. Rabilloud, *J. Phys. Chem. C*, 2019, **123**, 6205–6212.
30 M. Shibuta, K. Yamamoto, T. Ohta, T. Inoue, K. Mizoguchi, M. Nakaya, T. Eguchi and A. Nakajima, *ACS Nano*, 2021, **15**, 1199–1209.
31 M. M. Wind, J. Vlieger and D. Bedeaux, *Phys. A*, 1987, **141**, 33–57.
32 M. Nakaya, T. Iwasa, H. Tsunoyama, T. Eguchi and A. Nakajima, *Adv. Funct. Mater.*, 2014, **24**, 1202–1210.
33 M. Nakaya, T. Iwasa, H. Tsunoyama, T. Eguchi and A. Nakajima, *Nanoscale*, 2014, **6**, 14702–14707.
34 M. Nakaya, T. Iwasa, H. Tsunoyama, T. Eguchi and A. Nakajima, *J. Phys. Chem. C*, 2015, **119**, 10962–10968.
35 I. Horcas, R. Fernández, J. M. Gómez-Rodríguez, J. Colchero, J. Gómez-Herrero and A. M. Baro, *Rev. Sci. Instrum.*, 2007, **78**, 013705.
36 M. Shibuta and A. Nakajima, *J. Phys. Chem. Lett.*, 2023, **14**, 3285–3295.
37 P. B. Johnson and R. W. Christy, *Phys. Rev. B: Solid State*, 1972, **6**, 4370–4379.
38 A. Richter and J. Sturm, *Appl. Phys. A: Mater. Sci. Process.*, 1995, **61**, 163–170.
39 P. C. Eklund, A. M. Rao, Y. Wang, P. Zhou, K. A. Wang, J. M. Holden, M. S. Dresselhaus and G. Dresselhaus, *Thin Solid Films*, 1995, **257**, 211–232.
40 M. L. Brongersma, N. J. Halas and P. Nordlander, *Nat. Nanotechnol.*, 2015, **10**, 25–34.
41 N. G. Bastús, J. Piella and V. Puntes, *Langmuir*, 2016, **32**, 290–300.
42 W. He, X. Huang, X. Ma and J. Zhang, *J. Opt.*, 2022, **51**, 142–153.
43 J. A. Scholl, A. L. Koh and J. A. Dionne, *Nature*, 2012, **483**, 421–427.
44 M. Shabaninezhad and G. Ramakrishna, *Plasmonics*, 2020, **15**, 783–795.

